PROBABILISTIC TSUNAMI HAZARD ASSESSMENT FOR NEAR-FIELD EVENTS

Alejandra Gubler[1] , Patricio A. Catalán[2] and Yutaka Hayashi[3]

Abstract

The present paper describes a methodology to incorporate uncertainty on tsunami hazard assessments, specifically within the framework of Tsunami Warning Systems based on databases of pre-computed scenarios. The method uses sub fault unitary sources to discretize the possible rupture domain, whose tsunami solutions are then linearly combined to generate time series at forecast points. Aggregation of all possible scenarios yields exceedance probability curves for wave height and arrival times, thus providing more information than traditional database procedures, without a significant computational cost and loss of accuracy. In this study the focus is set on the uncertainty in epicentral location relative to the rupture and results are verified against data from the 2010 Maule Tsunami in Chile, with good qualitative agreement. The procedure could be easily expanded to include other uncertainty sources, and also can be coupled to inversion techniques if real time data becomes available.

Keywords: Probabilisitic Tsunami Hazard Assessment, Forecast Database, Tsunami Modeling

1. Introduction

Near field tsunami events pose a significant challenge for Tsunami Warning Systems (TWS), owing to the very short lapse between tsunami generation and its arrival to the coast. For example, for the February 2010 Mw8.8 Chile tsunami, the first waves arrived within 20 minutes. In order to respond effectively in issuing warnings and alerts, an accurate estimation of the tsunami hydrodynamic characteristics is required. However, the short time to obtain both an estimation of the seismic event and model results for tsunami propagation precludes the use of modeling in real time, at least with current computing capabilities.

As a response to this challenge, forecast systems have taken advantage to the idle time between tsunami events to prepare a database of pre-computed tsunami scenarios. Such databases have been implemented in several countries, and the operational methodology can be broadly categorized under two schemes. First, the method used by the National Oceanic and Atmospheric Administration of the United States uses both seismic and tsunami information to estimate the characteristics of the tsunami source, which is then used to propagate to the area of interest a linear combination of previously computed unitary tsunami solutions. This method is most suitable for far field scenarios when tsunami characteristics can be obtained and validated at far field data points (buoys), hence reducing uncertainty (Gica et al., 2008). On the other hand, the method originally developed by the Japan Meteorological Agency of Japan, and now also at Indonesian Tsunami Warning Center among others, use only the seismic information to enter a table look-up procedure, on which pre-computed values of similar seismic scenarios are interpolated to find the best match with the actual event, and next tsunami amplification characteristics at the coast are estimated to determine the tsunami hazard. This approach is more suitable to near field events because relies mostly on seismic data. If tsunami observations are available, they can be used to improve the solution through assimilation, and update the hazard assessment.

However, the closeness of the fault zone to the coast induces a significant reduction in response time if tsun

1 Departamento de Obras Civiles, Universidad Técnica Federico Santa María, Av. España 1680, Valparaíso, Chile. alejandra.gubler@alumnos.usm.cl

2 Departamento de Obras Civiles, Universidad Técnica Federico Santa María,. patricio.catalan@usm.cl

3 Meteorological Research Insititute, Japan. yhahashi@mri-jma.go.jp

ami data are to be used, for instance in the case of Chile. Hence, reliance on the seismic data is, to date, the only feasible option for an operational near-field TWS for places with such characteristics. The seismic dat a required comprises hypocentral location (latitude, longitude, and depth), and the moment magnitude of th e earthquake. In table-lookup procedures, multiple scenarios (combinations of feasible values of these quan tities) are used to generate the tsunami initial waveform based on the Okada (1985) estimation of the coseis mic crustal deformation, which assumes that the epicenter is located at the center of the rupture zone. Whil e inaccuracies in the relative position of the epicenter to the actual rupture zone might not be relevant for th e far field, they may lead a certain degree of variability in the tsunami characteristics for near field situation s. As an example, the epicenter for the 1960 Mw9.5 earthquake is located at the north-east end of the actual rupture zone (Moreno et al., 2009), which may have prompted an overestimation of the hazard in Central C hile if the standard approach had been used. On the other hand, the epicenter of the 2010 event was located very close to the coast and slightly southward relative to the center of the rupture zone (Vigny et al., 2011). Simulations using the Okada model for this configuration lead to an underestimation of the tsunami hazard over the same region. This variability suggests that the epicenter location is not a good descriptor of the rup ture zone and might play a secondary role in hazard estimation. The obvious solution is to have as soon as possible detailed information of the actual rupture geometry and associated displacements, but such solutio ns are still time consuming and may not be available within the time required for an effective warning.
To reduce the uncertainty relative to the epicenter location in the case of near coastal sources, Japan applies the Maximum Risk Method, which defines a rectangular uncertainty area centered at the estimated epicenter, and then select all simulation points (epicenter of the scenario fault) which are inside the rectangle. It chooses the worst case for each forecast point, based on the modeled maximum wave height and the earliest arrival time for each location. Improbable simulation points can be excluded using real time data at tide gages (Kamigaichi, 2011). In the Indonesian approach, an elliptical uncertainty area around the measured epicenter is defined, upon which a selection of all scenarios within the ellipse is performed based on seismic data. After choosing the best fitting scenarios (compared to real data using GPS measurements), the one with the largest moment magnitude within the range (Mw-0.5,Mw+0.3) is selected and the maximum amplitudes and arrival times at the Indonesian coasts are estimated. (Rakowsky et al., 2013, in press).

In the present work we extend these procedures by defining as a probable tsunami scenario any event whose rupture zone includes the estimated epicenter, yielding an uncertainty area four times larger than the estimated rupture area and an unspecified number of scenarios. As a first step, this allows us to estimate the expected variability in tsunami parameters due to the uncertainty in epicenter location. Next, aggregation of all possible scenarios leads to the exceedance probability of a target wave height value over the total number of simulations given the measured earthquake epicenter, which can then be used to provide more meaningful information than the worst-case scenario in the hazard estimation.

For the present work, we focus our analysis on the 2010 event as proof-of-concept; therefore, we analyze all unit sources within its rupture domain. First, to verify the use of linear combinations, results are compared against tsunami model results using COMCOT (Wang, 2009) driven by the fault parameters estimated by the United States Geological Survey (Hayes, 2010). Next, we assess the procedure outlined above as if it had been used for the same event as a forecast tool. Finally, we discuss the benefits of the approach presented herein and future work.

2. **Methodology**

The seismic rupture process is complex to model, and the resulting coseismic crustal deformation and its associated displacement of the ocean surface are not trivial to estimate. In order to maximize the evacuation time for the population, hazard assessment procedures need to take advantage of the information available as it is produced. Among these, seismic parameters such as its moment magnitude and epicentral location can be obtained in relatively short time. Although this may not be the most complete information to characterize a seismic event, the very short lapse between tsunami generation and its arrival to the coast makes it useful information to begin the hazard assessment procedure. For locations where this time is very short, it remains as the only feasible option for an operational near-field TWS. The low level of information provided by these parameters makes necessary to assume some model to estimate the coseismic crustal deformation and the initial tsunami waveform, usually by means of the e*lasticity theory* of dislocations proposed by Okada (1985). This allows calculation of the free surface displacement,

strains and tilts for a given a rectangular fault geometry (length L width W, depth d, strike ϕ, and dip δ) and three components of dislocation amplitude (rake λ, slip u and open). However, real fault mechanisms do not have uniform slip distribution, and it is then reasonable to use a methodology that allows using an heterogeneous fault model if that level of information becomes available.

For the Okada model to be used, aside from the epicentral location and moment magnitude, other fault parameters are required which can be estimated from the characteristics of the subduction zone. In addition, scaling laws are required to relate the fault length, width and slip to the moment magnitude of the earthquake. We use specifically the scaling law by Papazachos et al. (2004) for dip-slip faults in subduction regions, because it included historical data from Chilean earthquakes on its derivation and also because it covers a wider range of moment magnitudes ($6.7 \leq Mw \leq 9.2$). The scaling laws is based upon the seismic moment Mo (dyn-cm)

$$Mo = \mu S u \qquad (1)$$

where μ is the shear modulus of the rocks, assumed to be 4.0×10^{11} dynes/cm^2, S the fault area and u the mean displacement during rupture. The relation between moment magnitude Mw and seismic moment is:

$$\log(Mo) = 1.5Mw + 16.1 \qquad (2)$$

Papazachos et al. (2004) found the following relations between fault length L (in km) and fault area S (in km^2) to moment magnitude Mw:

$$\log(L) = 0.55Mw - 2.19; \quad \sigma = 0.8 \; ; \quad 6.7 \leq Mw \leq 9.3 \qquad (3)$$

$$\log(S) = 0.86Mw - 2.82; \quad \sigma = 0.25 \; ; \quad 6.7 \leq Mw \leq 9.2 \qquad (4)$$

Combining Eqs. (3) and (4) yields the fault width W (in km),

$$\log(W) = 0.31Mw - 0.63 \; ; \quad 6.7 \leq Mw \leq 9.2 \qquad (5)$$

Eqs. (1) – (4) give the following relation between the mean displacement, u (in cm)

$$\log(u) = 0.64Mw - 2.78 \qquad 6.7 \leq Mw \leq 9.2 \qquad (6)$$

Hence, the fault parameters for a given moment magnitude Mw, namely fault length L, fault width W, and mean displacement u, are obtaining using relations (3), (5) and (6) respectively.

On the other hand, recent earthquakes in Chile have highlighted that the epicenter location is not necessary centered on the fault, as proposed by the Okada model, a situation that can affect the quality of the assessment if a deterministic approach is used. Due to this uncertainty, we define as a probable tsunami scenario any event whose rupture zone includes the estimated epicenter. This means that the estimated epicenter could not be necessarily located close to the center of the fault, and is even possible that the epicenter is located close to the borders of the fault. Therefore, we set up an uncertainty rectangle centered at the estimated epicenter with dimensions of $2L$ in length and $2W\cos(\delta)$ wide projected in the horizontal plane, in order to cover all possible scenarios. In Fig. 1 the uncertainty rectangle is shown, and pink rectangles indicate sample scenarios to illustrate the relative location of the epicenter in the different faults. The orientation of the uncertainty rectangle is along the trench, which is often the orientation of the events in the Chilean case. However, this procedure would lead to the calculation of several deterministic scenarios, which can be a time consuming endeavor not suitable for a TWS.

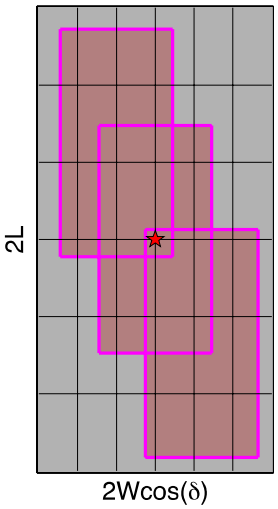

Figure 1. Seismic uncertainty rectangle and its associated faults. The red star denotes the estimated epicenter. The grey rectangle delimits the uncertainty area and it is centered at the epicenter, its dimensions being *2L* in length and *2Wcos(dip) wide*, projected in the horizontal plane. The smaller pink rectangles indicate sample scenarios that include the epicenter. Grid in black denotes the unit sources domain.

As an alternative, we adapt the methodology used by NOAA on its project SIFT (Gica et al., 2008), by subdividing the estimated source domain into several pre-defined earthquakes sources, henceforth named unit sources. A similar approach have also been used for instance in inversion algorithms with the objective to improve characterization of the source for far field forecasting, but they require real time data from sensors which might not be available everywhere (e.g. Wei et al., 2003; Sanchez and Cheung, 2007). We set unit sources of moment magnitude of *Mw* 7.0 and slip value of 1 m., yielding fault dimensions 40 km long and 20 km wide. The *Mw* 7.0 value is less than the value used by NOAA (*Mw* 7.5), owing to the consideration that lower values of moment magnitude will not produce a significant tsunami, and magnitudes over *Mw*7.0 yield unit sources of large dimensions compared to the actual geometries, affecting the representation of events of any magnitude. These units sources are shown in Fig. 1 by thin black lines.

For all unit sources, a synthetic tsunami was generated based on the crustal deformation derived from an Okada model and assuming the initial waveform equal to the seafloor deformation. The tsunami propagation was modeled using COMCOT (Cornell Multi-grid Coupled Tsunami model), using the linear approach based on Shallow Water Equations. The nonlinear terms were neglected in the modeling with the purpose of combining linearly the unitary solutions and also because small differences in the results of the r egional propagation considering the nonlinear effects were found during test runs. For the purpose of this method, only the initial tsunami waveform and the time history record of the free surface at the virtual buoys are stored in a database for all unit sources, resulting in a small and manageable database.
Consequently, the subdivision of the earthquake source domain allows reproducing the initial seafloor deformation (initial tsunami waveform) by combining linearly the corresponding unit sources to match the expected deformation. As mentioned before, this is possible due to the linearity of the generation and propagation dynamics of the tsunami.

We define a possible scenario and we define as *n* the total amount of unit sources contained into the expected rupture area. We define the following equation:

$$\eta_{SC}^{i} = \left[\eta_{US_1}^{i} | \eta_{US_2}^{i} | \ldots | \eta_{US_j}^{i} | \ldots | \eta_{US_n}^{i}\right] * x^{i} \qquad (7)$$

In which η^{i}_{sc} is the initial tsunami waveform of the i^{th} scenario, η^{j}_{US} the initial tsunami waveform of the j^{th} unit source over a total of n unit sources contained into the rupture area, and x^{i} the unknown solution vector yielding the vertical displacement of the unit sources, which is obtained solving Eq. (7). This constitutes a simple system of equations whose solution is found by minimizing the least-squares error.

Determination of x^{i} allows estimation of the initial tsunami waveform η^{*j}_{sc} at locations of interest

$$\eta^{*\,i}_{sc} = \left[\eta^{i}_{US_1} | \eta^{i}_{US_2} | \ldots | \eta^{i}_{US_j} | \ldots | \eta^{i}_{US_n}\right] * x^{i} \tag{8}$$

Similarly, we define h^{i}_{k} as the estimated time history record of the free surface resulting from i^{th} scenario located at k^{th} virtual buoy

$$h^{*\,i}_{k} = \left[h^{i,k}_{US_1} | h^{i,k}_{US_2} | \ldots | h^{i,k}_{US_j} | \ldots | h^{i,k}_{US_n}\right] * A^{i} \tag{9}$$

On which h^{i}_{k} is the estimated time series of the free surface of the i^{th} scenario located at the k^{th} virtual buoy, and $h^{i,k}{}_{USj}$ the time series of the j^{th} unit source over a total of n contained into the rupture area of the i^{th} scenario at the k^{th} virtual buoy.

This procedure is repeated over all possible scenarios, resulting in time series for each one of them. From the database is possible to extract the maximum wave height of the waves and its arrival times to the coast for all locations. Aggregation of all possible scenarios leads to the exceedance probability of a target wave height value given the estimated earthquake epicenter for each location.

Verification

In order to verify the methodology, we focus in the February 27, 2010 Maule earthquake and tsunami. Therefore, we define twelve rows and 22 columns of unit sources, yielding a total of 264 unit sources within a 880 km x 240 km source domain, centered in the epicenter of the 2010 event near Cobquecura, as shown in Fig 2, where the bathymetry and fault location are also shown. The epicenter is located slightly southward relative to the center of the rupture zone (Vigny et al., 2011).

The estimated fault length and width were found to be 500 and 120 km respectively, and the slip up to 15 m. The area of study covers the central region of Chile (from 29°S to 41°S and 69°W to 77°W) and 13 virtual tidal gauges were located along the coast, some of them close to existing gauges, like in Valparaiso (71.625ºW, 33.027°S) and Talcahuano (73.106°W, 36.695°S), in order to compare with real measurements of the tsunami wave height. The bathymetry/topography data used was obtained from GEBCO with 30 seconds of arc resolution. For the tsunami modeling using COMCOT, two extra grids were nested to the main grid (In Valparaiso and Talcahuano), both with a resolution of 10 seconds of arc. The tsunami modeling for all unit sources was integrated for 5 hours, using a time step of 1 s.

The unit sources are set up aligned to the trench, and the strike, dip and rake angles are determined by the characteristics of the Nazca/South American subduction zone, which are fairly constant along the area of interest (Sanchez and Cheung, 2007). Thus, the strike angle was set to 18°, the value for the dip was taken as 18°, and for the rake angle as 112°. Finally, the depth of the top margin of the fault was set to 6.2 km.

The dimensions of probable scenarios of magnitude Mw8.8 are obtained using the scaling law (Papazachos et al., 2004), yielding a rupture length of 450 km, width of 140 km and slip of 7.1 m. Similar parameters were used by Yamazaki and Cheung (2011), with a rupture area of 540 km by 200 km with an average slip of 4.2 m.

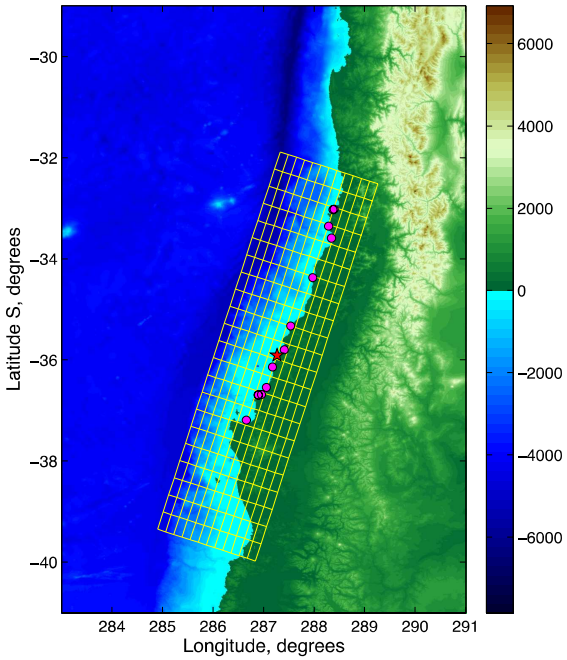

Figure 2. Mw7.0 unit sources covering the rupture zone of the 2010 Chilean Earthquake (yellow grid). The red star denotes the estimated epicenter. Pink dots denote the 13 virtual tidal gauges located along the coast. Colormap denotes the vertical terrain elevation relative to the mean sea level, in meters.

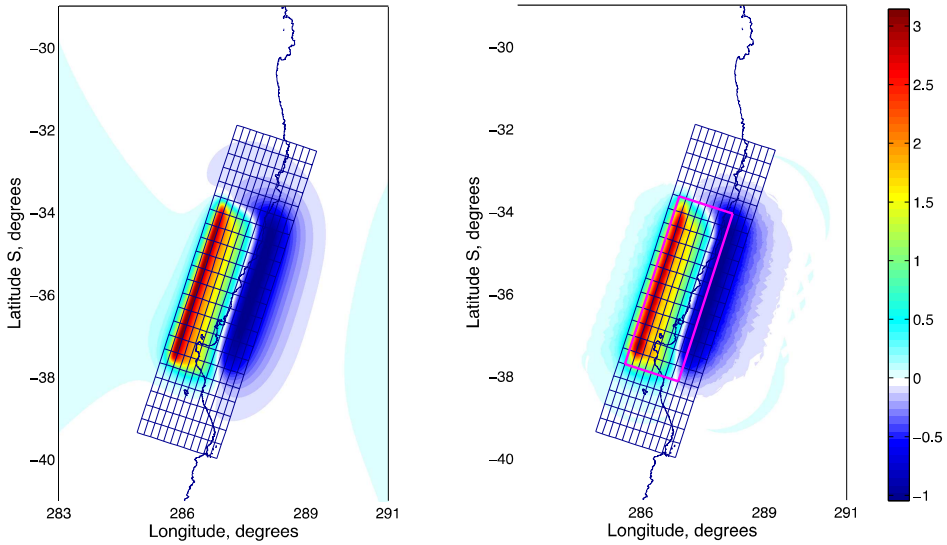

Figure 3. Reconstruction of the seafloor deformation combining linearly unit sources involved. Seafloor deformation of a probable scenario using Okada model (left panel). Reconstructed seafloor deformation by a linear combination of unit sources within pink rectangle (right panel). Colormap is vertical displacement in meters.

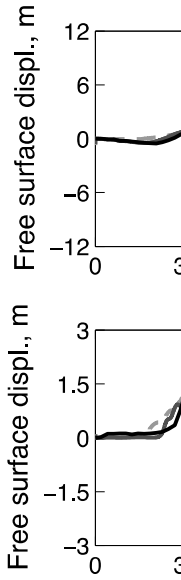

Figure 4. Tide gage records and corresponding model results in Talcahuano (top panel) and Valparaiso (bottom panel). Black line denotes the r

In Fig. 3, a sample of the computation procedure is shown. On the left panel, the crustal deformation with uniform slip centered at the actual epicenter is presented. The right panel shows the its reconstruction based on the solution of Eq. (7), showing a good agreement.

Next, the times series of the tsunami at points of interest are calculated using Eq. (9). In Fig. 4, top panel, the comparison at Talcahuano is presented, where we have also included the only tide gage record available in the near field. Also, the deterministic solution using as input the heterogeneous slip distribution obtained by Hayes (2010) is shown. Fig 4b. shows the same data, but this time for the bay of Valparaiso, which is located northward from the rupture zone and can be considered as far field.
It is of note that the tidal gage at Talcahuano was left exposed during the withdrawal of first wave, and the second wave took it away, reducing the data available for comparison. Nevertheless, the arrival and wave height for the first wave is fairly well reproduced by both the heterogeneous model and the linear combination presented here, despite the gage being located in relatively shallow water. The arrival time is also well retrieved. Regarding to the amplitude of the second wave, there are some difference between our method and the results of the heterogeneous model, and for these two simulations the second wave arrives approximately 4 minutes before to the real data. Subsequent waves show significant differences between the two simulations and can not be validated with real data.
For the case of Valparaiso (Fig. 4, bottom panel), the difference between solutions of the methodology and the real data is more significant. The amplitude of the first wave is underestimated, but its phase is well reproduced. There are difference respects to the amplitude and arrival times of the waves for both simulations. This could be due to the gage being located inside a harbor that is not well represented by the coarse resolution used here. A qualitative comparison with results from Yamazaki and Cheung (2011) who used similar bathymetric sources shows good agreement with results from our method.

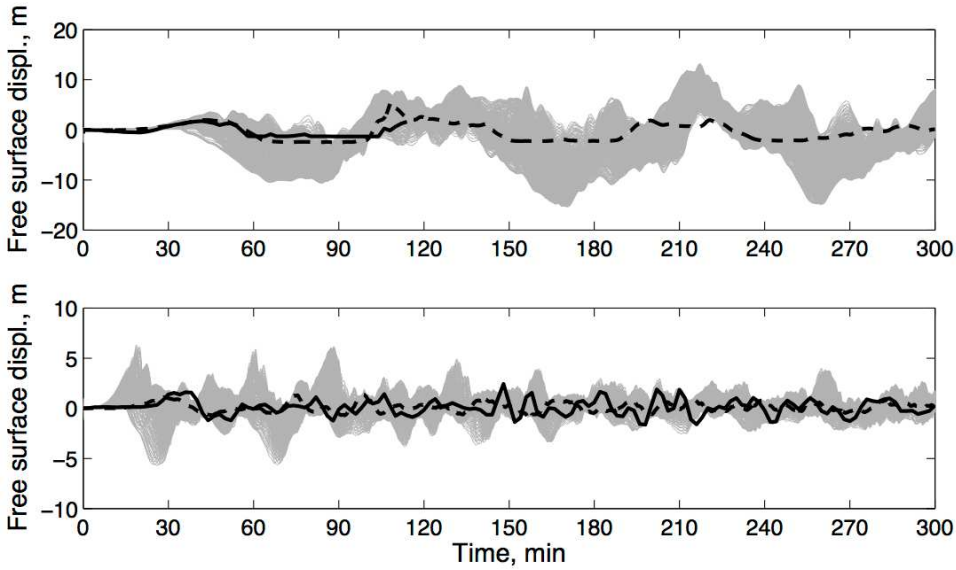

Figure 5. Synthetic time series of wave height of all possible scenarios against real data. Grey lines denotes the results of linear combination of unit sources of all scenarios. Solid black lines denotes the real tidal gauge record. Dashed line denotes results using heterogeneous seismic data.

As a result of this verification, it can be seen that the amplitudes and phases of the waves can strongly vary from one simulation to another, but in general, the characteristics of the first two waves appear to be well reproduced. Therefore, in constructing exceedance probability curves of the maximum wave amplitude over all possible scenarios we will focus on the first two waves for each scenario.

In Fig. 5, we present the resulting time series for all possible scenarios for the tide gage at Talcahuano, where 473 scenarios were generated. It can be seen that there is some significant variability on the resulting tsunami time series due to the uncertainty in the epicenter. Certain scenarios reduce the arrival time to just a few minutes. Variability is also large between the extreme of the free surface elevation series.

The maximum wave amplitude is defined as the maximum wave height between zero crossings. High frequency zero crossings may lead to small wave heights and introduce bias in the estimation of arrival times. This also affects characterization of what constitutes the first and subsequent waves. A threshold value can be defined to minimize this effect, as shown below.

In order to facilitate the analysis, the data gathered is presented in terms of accumulated exceedance probability by counting the number of scenarios that exceed a given height level, or arrival time, over the total number of scenarios. The results are shown in Fig. 6 for Talcahuano and Valparaiso, respectively where two sets of lines are shown. Black lines represent results where scenarios yielding wave heights less than 20 cm have been removed from the analysis while raw distributions are shown in light grey lines for reference. The first wave at Talcahuano (solid lines) shows a relatively uniform distribution of values, ranging from a few centimeters up to 3.8 m. and more than 30% of the scenarios can exceed 2 m at the point of interest. The second wave shows a different behavior, where less than 25 % of the simulations yield less than 2 m and more than 50% of the combinations predict wave heights exceeding 6 m, and some scenarios can exceed 8 m. On the other hand, in Valparaiso, the distributions show just a small fraction of the events (less than 15%) exceeding 2 m for either wave.

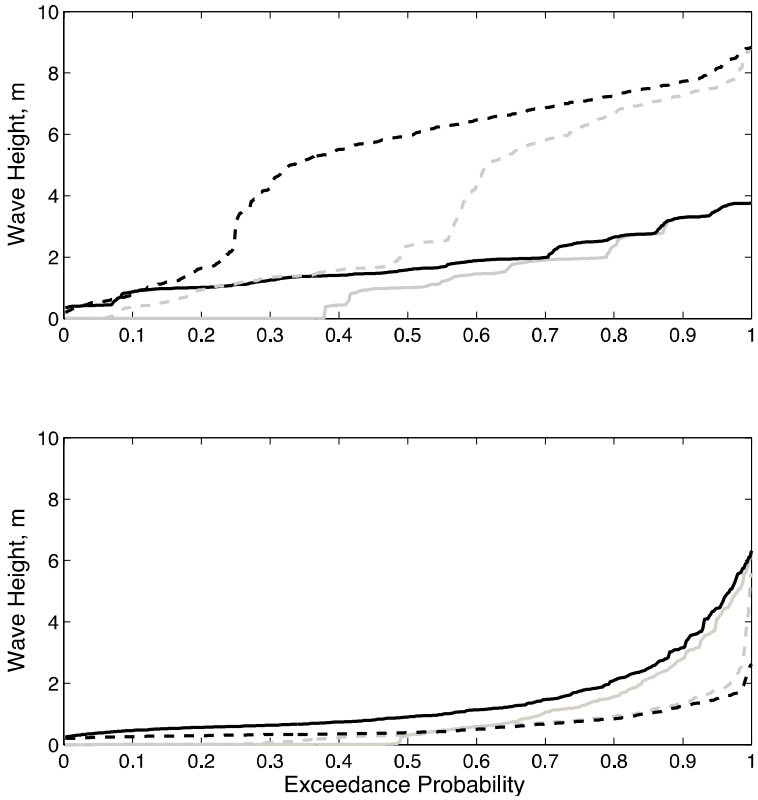

Figure 6. Exceedance probability of wave height over the total number of simulations for the first two waves in Talcahuano (top panel); and Valparaiso (bottom panel). Black lines denote filtered data and gray lines unfiltered data. Solid and dashed lines denote first and second wave, respectively.

Discussion

The methodology presented shows the potential to be used as to be a fairly good and quick tool in tsunami hazard assessment for near-field events to be used during emergency, especially useful when real time data measurements are not available. Unlike existing inversion algorithms (e.g. Wei et al, 2003; Sanchez and Cheung, 2007) the use of sub fault unit sources is used to solve a forward problem as a way to address the uncertainty in the location of the epicenter relative to the actual rupture. Other TWS such as the Japanese and Indonesian tackle this uncertainty by defining an interrogation domain larger than the estimated rupture zone, and then use the worst scenario to trigger the decision process. However, those databases are built on a finite number of scenarios (magnitudes) at specific control points. The smaller spatial extent of the sources used by the method presented here allows a larger number of combinations to be included in the assessment, thus allowing for the possibility of including a configuration leading a more destructive event. Alternatively, it also allows for quick estimation of an event of magnitude exceeding the database.

We tested the methodology with the 2010 event, and results are qualitatively consistent with the observed tsunami characteristics. For example, in Talcahuano, a large number of the possible scenarios yield large wave heights at the tide gage, whereas in Valparaiso, a smaller fraction of scenarios yields potentially destructive waves. This information is condensed in exceedance probability curves, which can be useful in the tsunami assessment process, depending on the purpose. If population evacuation is the objective, extreme values can still be the relevant quantity to trigger warning or alarm procedures, thus taking a conservative approach. However, this kind of approach can also be relevant for less extreme events which, although generating tsunamis, their effect could be relevant for port operations or coastal infrastructure, where a less conservative approach could be used.

Moreover, this method can be applied not only using dislocation models (uniform slip) and to simple crack models (constant stress drop) but also to stochastic slip models (heterogeneous stress drop) as the models presented by Geist (2012) for the 2010 Chile event. If geological and seismical information are available,

the location of macro asperities can be included to model stochastically zones of larger slip and deformation, by simply including a larger number of simulations.

It is noteworthy that the methodology proposed can be integrated in databases of pre-computed scenarios, adding an extra layer of information to be taken into account. For databases in development, sometimes the number of scenarios required is very large under the traditional methodology, and the present proposal allows for a system that can be implemented in less time. Finally, once a database of unitary sources is set up, it allows for the quick development of inversion techniques once real time data becomes available.

Conclusions and Future Work

A probabilistic method to evaluate the tsunami hazard for near field events is presented on which uncertainty is included by quickly computing a large number of scenarios given low-level seismic information. Specifically, the methodology presented here addresses the uncertainty in locating the epicenter relative to the rupture area. It is shown there is large variability in estimations of the wave height and arrival times at forecast points, which is summarized in exceedance probability curves. These curves provide relevant information for tsunami hazard assessment at various levels, depending on the mitigation objective.

The method relies in linear superposition of events in the near field. While results deviate from measured data for long simulation time, the first couple of waves are generally well reproduced. In addition, the methodology allows for more flexibility in incorporating extreme events or other sources of uncertainty such as non-homogenous slip distributions, and also allows for the possibility to couple it in inversion techniques if suitable real time data becomes available.

Future work regarding the methodology includes improving the forecast for longer simulations. In addition, we will explore inclusion of other sources of uncertainty such as non-homogeneous slip distributions and tide levels. On the other hand, site-specific analysis of threshold values for the relevant variables can be useful in determining levels to trigger the different stages of tsunami warning.

Acknowledgements

The authors would like to thank JICA and JST and their SATREPS Initiative "On Enhancement of Technology to Develop Tsunami-Resilient Community"; and CONICYT Grants FONDEF/D11i1119 and FONDAP/15110017.

References

Geist, E. L. (2012), 'Near-Field Tsunami Edge Waves and Complex Earthquake Rupture', *Pure and Appl. Geoph.*, 1--17.

Gica, E.; Spillane, M. C.; Titov, V. V.; Chamberlin, C. D. & Newman, J. C. (2008), 'Development of the Forecast Propagation Database tor NOAAs Short-term Inundation Forecast For Tsunamis (SIFT)', NOAA Technical Memorandum OAR PMEL-139

Hayes (2010). Finite fault model. Updated Result of the Feb 27, 2010 Mw 8.8 Maule, Chile Earthquake. <http://earthquake.usgs.gov/earthquakes/eqinthenews/2010/us2010tfan/finite_ fault.php> .

Kamigaichi, O., (2011), Tsunami forecasting and warning, in *Extreme Environmental Events*, Springer, Meyers, R. A., ed., pp. 982--1007.

Moreno, M. S.; Bolte, J.; Klotz, J. & Melnick, D. (2009), 'Impact of megathrust geometry on inversion of coseismic slip from geodetic data: Application to the 1960 Chile earthquake', *Geophysical Research Letters* **36**(16), L16310.

Okada, Y. (1985), 'Surface deformation due to shear and tensile faults in a half-space', *Bulletin of the seismological society of America* **75**(4), 1135--1154.

Papazachos, B.; Scordilis, E.; Panagiotopoulos, D.; Papazachos, C. & Karakaisis, G. (2004), 'Global relations between seismic fault parameters and moment magnitude of earthquakes', *Bull. Geol. Soc. Greece* **36**, 1482--1489.

Rakowsky, N.; Androsov, A.; Fuchs, A.; Harig, S.; Immerz, A.; Danilov, S.; Hiller, W. & Schrıter, J. (2013), 'Operational tsunami modelling with TsunAWI - recent developments and applications', *Nat. Haz. & E S Sci* in press.

Sánchez, A. & Cheung, K. F. (2007), 'Tsunami forecast using an adaptive inverse algorithm for the Peru-Chile source region', *Geophysical Research Letters* **34**(13), L13605.

Vigny, C.; Socquet, A.; Peyrat, S.; Ruegg, J.-C.; Metois, M.; Madariaga, R.; Morvan, S.; Lancieri, M.; Lacassin, R.; Campos, J. & et al. (2011), 'The 2010 Mw 8.8 Maule Megathrust Earthquake of Central Chile, Monitored by GPS', *Science* **332**(6036), 1417--1421.

Wang, X. (2009). User Manual for COMCOT version 1.7 (first draft). Cornell University.

Wei, Y.; Cheung, K.; Curtis, G. & McCreery, C. (2003), 'Inverse Algorithm for Tsunami Forecasts', *Journal of Waterway, Port, Coastal, and Ocean Engineering* **129**(2), 60--69.

Yamazaki, Y. & Cheung, K. F. (2011), 'Shelf resonance and impact of near-field tsunami generated by the 2010 Chile earthquake', *Geophysical Research Letters* **38**(12), L12605.